Int J Adv Manuf Technol (2011) 55:883–889
DOI 10.1007/s00170-010-3139-8

ORIGINAL ARTICLE

Prediction of simultaneous dynamic stability limit of time–variable parameters system in thin-walled workpiece high-speed milling processes

Qinghua Song · Xing Ai · Weixiao Tang

Received: 11 May 2010 / Accepted: 29 December 2010 / Published online: 20 January 2011

Abstract A method for predicting simultaneous dynamic stability limit of thin-walled workpiece high-speed milling process is described. The proposed approach takes into account the variations of dynamic characteristics of workpiece with the tool position. A dedicated thin-walled workpiece representative of a typical industrial application is designed and modeled by finite element method. The curvilinear equation of modal characteristics changing with tool position is regressed. A specific dynamic stability lobe diagram is then elaborated by scanning the dynamic properties of workpiece along the machined direction throughout the machining process. The results show that, during thin-walled workpiece milling process, material removing plays an important part on the change of dynamic characteristics of system, and the stability limit curves are dynamic curves with time–variable. In practical machining, some suggestion is interpreted in order to avoid the vibrations and increase the chatter free material removal rate and surface finish. Then investigations are compared and verified by high-speed milling experiments with thin-walled workpiece.

Keywords Time–variable parameters system · Milling chatter · Dynamic stability limit · Finite element method

Q. Song (✉) · X. Ai · W. Tang
Key Laboratory of High Efficiency and Clean Mechanical Manufacture, Ministry of Education, School of Mechanical Engineering, Shandong University,
Ji'nan, China
e-mail: ssinghua@sdu.edu.cn

X. Ai
e-mail: aixing@sdu.edu.cn

W. Tang
e-mail: tangwx@sdu.edu.cn

1 Introduction

High-speed milling process is a highly demanding operation because of the high temperatures and stresses generated at the chip–tool and workpiece–tool interface due to large metal removal rates, in which chatter stability is one of the most common detrimental phenomenon and major obstruction toward achieving automation, higher productivity, and better surface finish that is directly subjected to the dynamic characteristics of system in high-speed milling processes [1]. Such dynamic characteristics are dependent on the milling process parameters, e.g., rotating speed of spindle, feed rate and direction, and depth of cut, and system parameters, e.g., mass, stiffness, damping, the number of teeth, and helix angle of cutter. Therefore, predictions of dynamic characteristics in high-speed milling processes are highly needed in order to achieve accurate chatter stability of milling system, ulteriorly achieve the optimizations of cutting conditions and cutter geometries, as well as online monitoring/adaptive control and vibration–suppression strategies [2].

Chatter vibration due to the dynamic interactions between tool and workpiece has been widely studied in the past century since Taylor first identified and described chatter in 1907. After the extensive work of Tobias [3] and Smith et al. [4], a constant time delay dynamics model for stability analysis of 2D milling process using harmonic balance and infinite determines was improved [5]. A linear discrete-time model was given to analyze stability in case of low radial immersion milling [6]. Stability of milling processes with variable time delays including the effect of feed ratio was presented using the semi-discretization method [7–9]. Based on the robust stability theorem, a novel method to predict chatter-free regions for machining processes was provided, by taking in account the unknown uncertainties and changing dynamics for machining [10]. All these authors present a fundamental

understanding of regenerative chatter as a feedback mechanism for the growth of self-excited vibrations due to variations in chip thickness and cutting force and subsequent tool vibration. These studies have led to graphic charts showing the stability information as a function of chip thickness and spindle speed. And the assumption was made that the dynamic characteristics of system did not change during the whole machining processes.

The focus of many recent works has been the phenomenon that the dynamic characteristics of system are changed during the whole machining processes, which have two important research embranchments. On the one hand, many authors have studied it through machine behavior [11–13], assuming a rigid workpiece. This assumption need to be considered in high-speed milling, where gyroscopic moments and centrifugal forces on both bearings and spindle shaft induce spindle, tool holder, and cutting tool speed-dependent dynamics changes. A finite element-based model of spindle, tool holder, and cutting tool which used Timoshenko beam theory was presented to obtain the frequency response of the system when gyroscopic terms were included [14]. It was shown that gyroscopic effects lower the critical depth of cut in high-speed milling.

On the other hand, workpiece behavior has been carried out assuming a rigid spindle tool set [15–17]. This assumption is relevant in specific industrial applications like very thin-walled aeronautical monolithic components or turbine blades. A mechanics-based model with impact nonlinearities was developed to explain that stiffness and damping nonlinearities due to intermittent cutting action have a pronounced effect on the dynamics of the workpiece which was assumed as a thin, isotropic, cantilevered plate with a single significant mode of vibration [18]. Bravo et al. [19] proposed considering such applications and suggested a method for obtaining a 3D stability lobe to cover all the intermediate machining stages. A similar approach was presented by combining the finite element method (FEM) representation of a flexible automotive workpiece and the spindle tool set [20, 21]. Thevenot et al. [22] introduced the dynamical behavior variation of the part with respect to the tool position in order to determine optimal cutting condition during the machining process and constructed a 3D stability lobe diagram. All above researches are based on the restrictive assumption that spindle-tool set dynamics do not change over the full spindle speed range.

During thin-walled workpiece milling process, material removing plays an important part on the change of dynamic characteristics of system, and the stability limit curves are dynamic curves with time–variable. The present work is undertaken to describe a method for predicting simultaneous dynamic stability lobe diagram (DSLD) of thin-walled workpiece high-speed milling process assuming a rigid spindle-tool set. The paper is organized as follows. In Section 2, a dynamic model with variable parameters system is introduced, including cutting force model, workpiece model, and workpiece dynamics depending on tool position. In Section 3, semi-discretization method is demonstrated to predict dynamic stability of variable parameters system. The experimental results and analysis are given in Section 4. Section 5 concludes the paper.

2 Dynamic model with time–variable parameters system

2.1 Cutting force model

The thin-walled workpiece can be considered to have a degree of freedom as shown in y direction assuming a rigid spindle tool set, as shown in Fig. 1. The symbol a_e is the radial depth of cut, and Ω is the constant rotational angular velocity (rad/s). Cutting forces excite the structure, causing dynamic displacement y of cutter in the normal (y) direction. The instantaneous chip thickness reads

$$h_{i,d}(t) = \cos(\varphi_i(t))[y(t-\tau) - y(t)] \tag{1}$$

where, $y(t-\tau)$ and $y(t)$ are the vibration displacements of the previous tooth and the current tooth. τ is time delay, $\tau=2\pi/(N\Omega)$. N is the number of teeth. $\varphi_i(t)$ is the location of the ith tooth

$$\varphi_i(t) = \Omega t + \frac{(i-1)2\pi}{N} \tag{2}$$

The instantaneous cutting force is proportion to the instantaneous chip thickness

$$f(t) = a_p d(t)[y(t-\tau) - y(t)] \tag{3}$$

where, a_p is the axial depth of cut; $d(t)$ is the specific cutting force factor

$$d(t) = \sum_{i=1}^{N} \{\delta_i(\varphi_i(t))\cos(\varphi_i(t))[-K_t \sin(\varphi_i(t)) + K_r \cos(\varphi_i(t))]\} \tag{4}$$

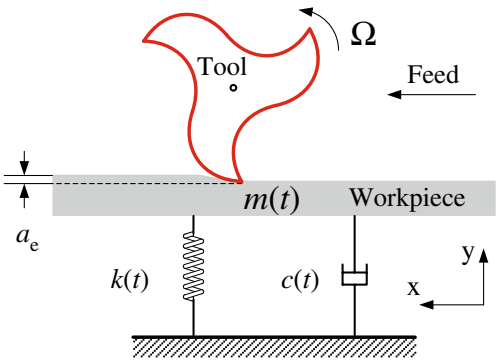

Fig. 1 Milling model for thin-walled workpiece

here, $d(t)$ is τ periodic, i.e., $d(t)=d(t+\tau)$. K_t and K_r are the tangential and radial cutting coefficients, respectively. $\delta_i(\varphi_i(t))$ a Heaviside step function that assumes a value one when the cutting tooth is engaged in cutting process and zero when the tool is out of the cut.

$$\delta_i(\varphi_i(t)) = \begin{cases} 1 & \varphi_{en} < \varphi_i(t) < \varphi_{ex} \\ 0 & \varphi_i(t) > \varphi_{ex}, \varphi_i(t) < \varphi_{en} \end{cases} \quad (5)$$

where, φ_{en} and φ_{ex} are enter angle and exit angle for tooth, respectively.

2.2 Workpiece model

The typical thin-walled workpiece is made from aeronautical aluminum alloy (7050-T7451), with physical properties: Young's modulus of elasticity E=70.3 GPa, density ρ=2,820 kg/m^3, and Poisson's ratio μ=0.33. The thin wall was down-milled in finishing with axial depth of cut, radial immersion of 0.6 mm, and feed rate of 0.1 mm/tooth. The workpiece dimensions chose for the study is a rectangular prism of 100×30×3 mm with a thin wall of 3 mm thickness and 30 mm height that can be found easily in the industry, for example an inner pocket wall.

During the finish machining of the part, dynamic properties evolve according to the tool position [20, 22]. In order to predict this evolution, a workpiece finite element method is established. The tool path is discretized over the whole workpiece and a modal analysis is carried out. Experimental modal characterization of the workpiece is carried out in order to adjust the FEM results to the real behavior of the part. These tests were made through a classic hammer test and mainly enable the damping ratio of the model to be readjusted.

The workpiece dynamic equations are established using a reduction of the FEM to specific master degrees of freedom using the Guyan algorithm. The workpiece is divided into 21 equidistant points, enabling an accurate workpiece dynamic prediction to be made throughout the machining process. The assumption is made that the workpiece FEM has a constant geometry during finishing machining due to the small amount of material removed.

2.3 Workpiece dynamic according to tool position

Assembling all the points mentioned before, the workpiece model is obtained. A modal analysis is carried out and allows the workpiece natural frequencies to be established at the different position of the cutter. The collected natural frequency data has been further used for finding the best fitting curve. The third degree polynomial equation is coming out to be best fitted curve with regression analysis coming equals to "1". Thus the equations of the first order natural frequencies for this case are given in Eq. 16.

Because the material removal rate (MRR) is small in one cutting process and the machining system is a lightly damped structures, it is assumed that the damping ratio of the workpiece does not change depending on tool position over the cutting process, i.e., $c(t)=c_0$ and $\zeta(t)=\zeta_0$. And the damping ratio of the workpiece is obtained from the initial state of the workpiece. The relationship between the modal mass and the modal damping is satisfied

$$m(t) = \frac{c(t)}{2\zeta(t)\omega_n(t)} = \frac{c_0}{2\zeta_0\omega_n(t)} \quad (6)$$

where, $\zeta(t)$ is the modal damping ratio, $\zeta(t)=c(t)/[2(m(t)k(t))^{1/2}]$; $\omega_n(t)$ is the natural frequency, $\omega_n(t)=[k(t)/m(t)]^{1/2}$; $m(t)$ is the modal mass; $c(t)$ is the modal damping; and $k(t)$ is the modal stiffness.

2.4 Milling system model with time–variable parameters

From the viewpoint of dynamical systems, thin-walled workpiece can be defined as the system that the dynamic characteristics change depending on the tool position, that is, the system considering the effect of machining process to the dynamic characteristics. The thin-walled workpiece milling processes is a time–variable parameters system, and the corresponding to the governing equation has the form

$$\ddot{y}(t) + 2\zeta(t)\omega_n(t)\dot{y}(t) + \omega_n^2(t)y(t) = \frac{f(t)}{m(t)} \quad (7)$$

Equation 7 is a linear periodic delay differential equation (DDE) with time–variable parameters. The two problems need to be considered for this kind of equations: one is time delay, the other is time–variable parameter.

3 Stability for time–variable parameters system

Semi-discretized technique is a well-known approximation technique in finite element analysis or in computational fluid mechanics for solving partial differential equations where the spatial coordinates are discretized while the time coordinates are unchanged [23, 24]. The method can be used to determine the stability of non-autonomous approximation of the monodromy matrix $\boldsymbol{\Phi}$ of a periodic DDE over the principal period T. Hereto, the period T is divided into k intervals of length Δt. The DDE is thereby approximated by a series of ordinary differential equations. The convergence of the method was established for a large class of DDEs appearing in engineering applications [24, 25].

The first step of semi-discretization is the construction of the time interval division $[t_j, t_{j+1}]$ of length Δt, $j \in Z$, of the time domain, so that $T=k\Delta t$, where the integer k is called as

approximation number. By decreasing Δt, that is, by increasing the approximation number k, the error decreases [24].

Introduce the integer m so that

$$m = \mathrm{int}\left(\frac{\tau}{\Delta t} + 0.5\right) \tag{8}$$

where, m is an approximation parameter regarding the length of the time delay. Details on how to treat this case can be found in reference [24].

In the jth interval for periodic time T, the period DDE (7) can be approximated with the following, autonomous ordinary differential equation

$$\ddot{y}(t) + 2\zeta_0\omega_{\mathrm{n},j}\dot{y}(t) + (\omega_{\mathrm{n},j}^2 + a_\mathrm{p}\frac{d_j}{m_j})y(t) = a_\mathrm{p}\frac{d_j}{m_j}y_{\tau,j} \tag{9}$$

where $y_{\tau,j} = \alpha y_{j-m+1} + \beta y_{j-m} \approx y(t_j + 0.5\,\Delta t - \tau) = y(t-\tau)$, $\omega_{\mathrm{n},j} = \frac{1}{\Delta t}\int_{t_j}^{t_{j+1}} \omega_\mathrm{n}(t)dt$, $d_j = \frac{1}{\Delta t}\int_{t_j}^{t_{j+1}} d(t)dt$, $m_j = \frac{1}{\Delta t}\int_{t_j}^{t_{j+1}} m(t)dt$.

By Cauchy transformation, Eq. 9 is written in the canonical form

$$\dot{\boldsymbol{Q}}(t) = \boldsymbol{W}_j\boldsymbol{Q}(t) + \boldsymbol{V}_j[\alpha\boldsymbol{Q}_{j-m+1} + \beta\boldsymbol{Q}_{j-m}] \tag{10}$$

where, $\alpha = \tau/\Delta t + 0.5 - m$, $\beta = m + 0.5 - \tau/\Delta t$, $\boldsymbol{W}_j = \begin{bmatrix} 0 & 1 \\ -(\omega_{\mathrm{n},j}^2 + a_\mathrm{p}\frac{d_j}{m_j}) & -2\zeta_0\omega_{\mathrm{n},j} \end{bmatrix}$, $\boldsymbol{Q}(t) = \begin{Bmatrix} y(t) \\ \dot{y}(t) \end{Bmatrix}$, $\boldsymbol{V}_j = \begin{bmatrix} 0 & 0 \\ a_\mathrm{p}\frac{d_j}{m_j} & 0 \end{bmatrix}$, $\boldsymbol{Q}_j = \boldsymbol{Q}(t_j) = \begin{Bmatrix} y(t_j) \\ \dot{y}(t_j) \end{Bmatrix} = \begin{Bmatrix} y_j \\ \dot{y}_j \end{Bmatrix}$.

For a given initial condition $\boldsymbol{Q}_j$, Eq. 10 can be solved in $t\in[t_j,\ t_{j+1}]$,

$$\boldsymbol{Q}_{j+1} = \boldsymbol{A}_j\boldsymbol{Q}_j + \boldsymbol{B}_j[\alpha\boldsymbol{Q}_{j-m+1} + \beta\boldsymbol{Q}_{j-m}] \tag{11}$$

where, $\boldsymbol{A}_j = \exp(\boldsymbol{W}_j\Delta t)$, $\boldsymbol{B}_j = (\exp(\boldsymbol{W}_j\Delta t) - \boldsymbol{I})\boldsymbol{A}_{j-1}\boldsymbol{V}_j$, $\boldsymbol{I}$ denotes identity matrix.

According to Eq. 11, a discrete map can be defined

$$\boldsymbol{z}_{j+1} = \boldsymbol{P}_j\boldsymbol{z}_j \tag{12}$$

where the $(m+2)$-dimensional state vector $\boldsymbol{z}_j$ is

$$\boldsymbol{z}_j = [y_j \quad \dot{y}_j \quad y_{j-1}\cdots y_{j-m}]^T \tag{13}$$

And the coefficient matrix $\boldsymbol{P}_j$ has the form

$$\boldsymbol{P}_j = \begin{bmatrix} A_{j,11} & A_{j,12} & 0 & \cdots & 0 & \alpha B_{j,11} & \beta B_{j,11} \\ A_{j,21} & A_{j,22} & 0 & \cdots & 0 & \alpha B_{j,21} & \beta B_{j,21} \\ 1 & 0 & 0 & \cdots & 0 & 0 & 0 \\ 0 & 0 & 1 & \cdots & 0 & 0 & 0 \\ \vdots & \vdots & \vdots & \ddots & \vdots & \vdots & \vdots \\ 0 & 0 & 0 & 0 & 1 & 0 & 0 \\ 0 & 0 & 0 & 0 & 0 & 1 & 0 \end{bmatrix} \tag{14}$$

Equation 12 makes the connection between states at time t_j and t_{j+1}. The connection between the states at t_0 and $t_0+k\Delta t=t_k$ is given by coupling of the coefficient matrices in each interval

$$\boldsymbol{\Phi} = \boldsymbol{P}_{k-1}\boldsymbol{P}_{k-2}\ldots\boldsymbol{P}_1\boldsymbol{P}_0 \tag{15}$$

The stability of (7) can be approximated by the Floquet transition matrix (15). Note that the integer k determines the number of matrices to be multiplied in (15), and m determines the size of these matrices.

4 Experimental results and analysis

Milling tests were performed on a high-speed machining center DMU-70 V, the maximum spindle speed of which is 18,000 rpm. Solid carbide cutter (coated by TiCN) with 12 mm of diameter and 30 degree helix angle (three flutes) was selected. The workpiece is clamped on the three-force component Kistler dynamometer, which is fixed on the table of the machining center. Three eddy current displacement sensors which measure the displacement in y direction are located on the workstation of the machine tool with equal space between, as shown in Fig. 2. The sensor may effectively measure micro-movements lower than 10 μm and its sensitivity curve is linear between 0 and 1 mm.

The experimental set-up is completed with three Kistler 5007 amplifiers, three eddy current displacement sensors, a force hammer, an electric charge amplifier, a filter, a microcomputer-based data acquisition system, and analytical software.

Initial experimental modal characterization of the workpiece was carried out in order to adjust the FEM results to the real behavior of the part. These tests were made by an impact hammer with an embedded piezoelectric force transducer and mainly enable the damping ratio of the model to be readjusted. The cutting coefficients were gained using linear regression of average cutting forces

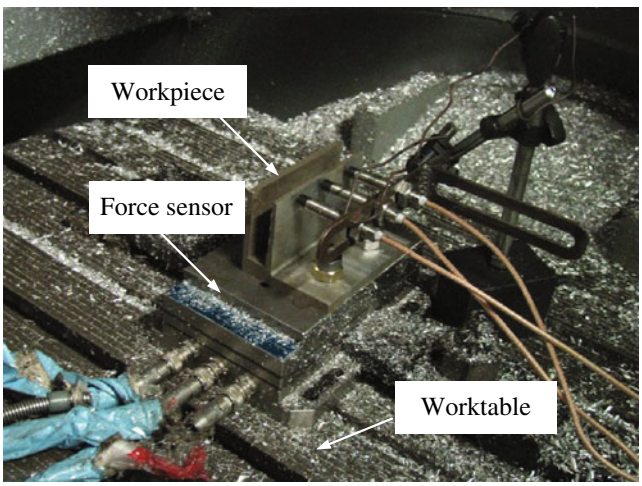

Fig. 2 Experimental setup

for several feed ratios in milling slot tests as shown in Table 1.

Without loss of generality, one cutting process (a_e is 5 mm, a_p is 0.6 mm, length of workpiece (x direction) is 100 mm, thickness is 3 mm) of workpiece is discreted. The 3D frequency response function (FRF) of workpiece depending on the tool position (or machining time) is obtained by the finite element method, as shown in Fig. 3.

By using the transform function theory and the least-squares method, the first modal natural frequency is expressed as

$$f_{n1}(x) = 1095 + 3.691x - 0.1361x^2 + 0.00101x^3 [\mathrm{Hz}] \quad (16)$$

The other modal parameters are also calculated by using (5). In Fig. 3, it is shown that, the FRF of thin-walled workpiece is changed with the tool position, and the FRF map is a dynamic curve with time–variable.

The 3D DSLD of thin-walled workpiece was determined for different spindle speeds and different tool positions by the method proposed in above section, as show in Fig. 4. The zones in the upper curved surface are unstable, and the zones under the curved surface are stable.

On the one hand, it can be seen that the graphic charts only determined by the "Spindle speed" axis and "Axial depth of cut" axis expresses the traditional stability lobes proposed in references [1–10]. It was assumed that the dynamic characteristics of system did not change during the whole machining processes. While, when the material removal is significant, the dynamic properties (natural frequencies, mainly) of the workpiece change according to the tool position. Thus, the 3D DSLD includes the variation of the dynamic parameters of the workpiece in third dimension of the stability lobes.

On the other hand, the graphic charts only determined by the "Tool position" axis and "Axial depth of cut" axis expresses the new stability lobes, which includes the variation of the dynamic parameters of the workpiece with a fixed spindle speed. Without loss of generality, three different spindle speeds (e.g., 14,000 rpm (case I), 15,000 rpm (case II), and 16,000 rpm (case III)) are selected. The DSLDs for these spindle speeds are shown in Fig. 5. In Fig. 5, the zones upper the curves are unstable, and the zones under the curves are stable. It can be seen that the variation of the natural frequencies of the workpiece during machining introduces a shift of the lobes along the spindle speed axis. Consequently, if this shift is rather significant, it is possible that no stable spindle speed exists throughout the machining process, e.g., case III in Fig. 5. Then, the spindle speed must be adjusted during machining in order to achieve a stable behavior of the workpiece.

Table 1 Initial modal parameters of workpiece and cutting coefficients

	m_0 (kg)	k_0 (N/m)	c_0 (Ns/m)	K_t (N/m^2)	K_r (N/m^2)
y	0.03	3.782×10^4	2.56	5.4×10^8	1.8×10^8

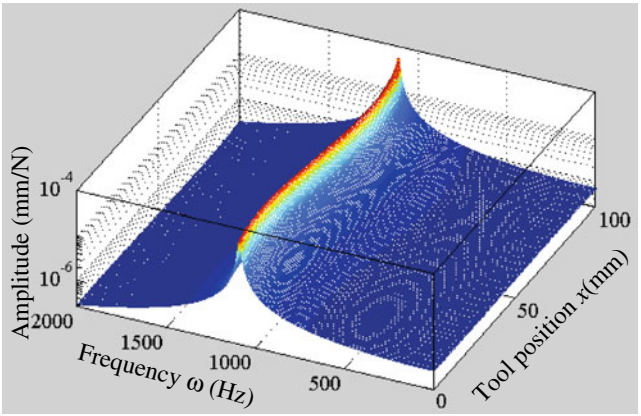

Fig. 3 Workpiece frequency response function map depending on the tool position

Down-milling experiments without coolant were performed with selected cutting parameters, feed per tooth (f_z) 0.1 mm, axial depth of cut (a_p) 5 mm, radial depth of cut (a_e) 0.6 mm, and the spindle speeds 14,000 rpm (case I), 15,000 rpm (case II), and 16,000 rpm (case III), respectively. Figure 6 is the photograph of machined workpiece. In Fig. 6, the regions denoted by the labels a–f is in accordance with those in Fig. 5. Comparing between Figs. 5 and 6, the well agreements can be observed between experimental results and numerical results. For milling process in 14,000 rpm case, the first half (e.g., a in Fig. 5) of the cutting process is unstable, and the cutting force is very large, while the second half process (e.g., b in Fig. 5) is stable. The results are also confirmed by the experimental photographs in Fig. 6. For the case of 15,000 rpm, it is contrary to the case of 14,000 rpm, the first half part is

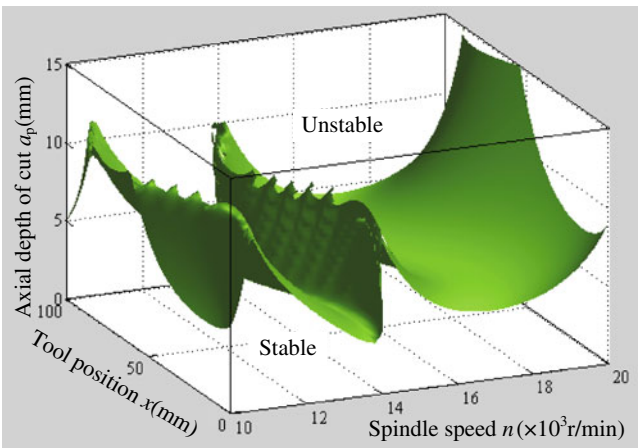

Fig. 4 Three-dimensional stability chart of thin-walled workpiece

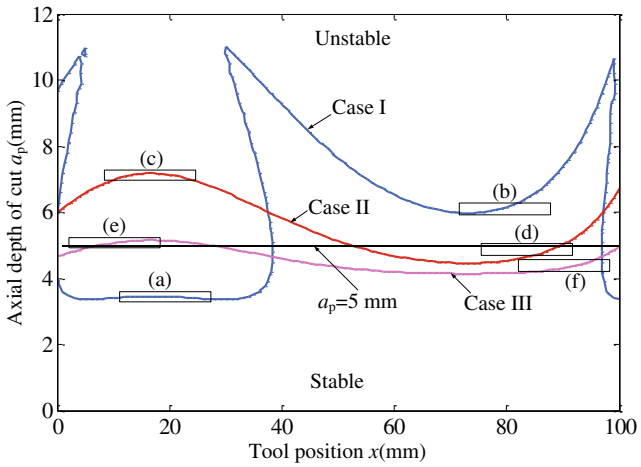

Fig. 5 Stable axial depth of cut depending on tool position. Case I, 14,000 rpm; case II, 15,000 rpm, case III, 16,000 rpm

stable, and the rest part is unstable. The whole process for the case 16,000 rpm is almost unstable, and the surface finish of machined workpiece is also very poor.

It is shown that, in order to avoid chatter vibration and increase the chatter free MRR and surface finish, cutting parameters during machining process of the thin-walled workpiece can be selected by using the dynamic stability lobes, which express the relationship between stability limits and tool position. For the case investigated in the paper, for example, the first half of cutting process is performed in 15,000 rpm, and the rest part is conducted in 14,000 rpm, when the other cutting parameters are fixed.

At the beginning of this article, two important assumptions were made, the one is that the tool is much more rigid than the workpiece; the other is that the tool is cylindrical with a constant pitch. In practice, the tool and the workpiece may be mobile. In this case, there can be coupling between them if the natural modes of the tool and the workpiece are close. The method presented is no longer valid directly and need to be updated. Meanwhile, if the end mill with variable pitch, e.g., end mill with variable helix angle, end mill with variable end-flute angle, used to improving stability against chatter for a certain speed ranges, the distribution of the cutting force is no longer uniform, and the resultant position of the cutting force changes. The author and co-authors have investigated the stability of end mill with variable pitch, and proposed an approach to design variable pitch end mill with high milling stability. The results will be published in The International Journal of Advanced Manufacturing Technology.

5 Conclusions

During workpiece machining, large quantities of material are removed in high removal rate conditions, with the risk of instability in the process. This unstable phenomenon, known as chatter, is quite critical since it causes poor surface finish and may lead to spindle, cutter, and part damage. In specific industrial applications like very thin-walled aeronautical structures or turbine blades, workpiece vibration is strongly dominant in comparison with spindle tool set vibration. Chatter vibration depends on the cutting conditions and also on the tool position along the machined thin wall. A method for predicting the DSLD of thin-walled workpiece milling process is described. The proposed approach takes into account the variations of dynamic characteristics of workpiece with the tool position. A specific DSLD is then elaborated by scanning the dynamic properties of workpiece along the machined direction

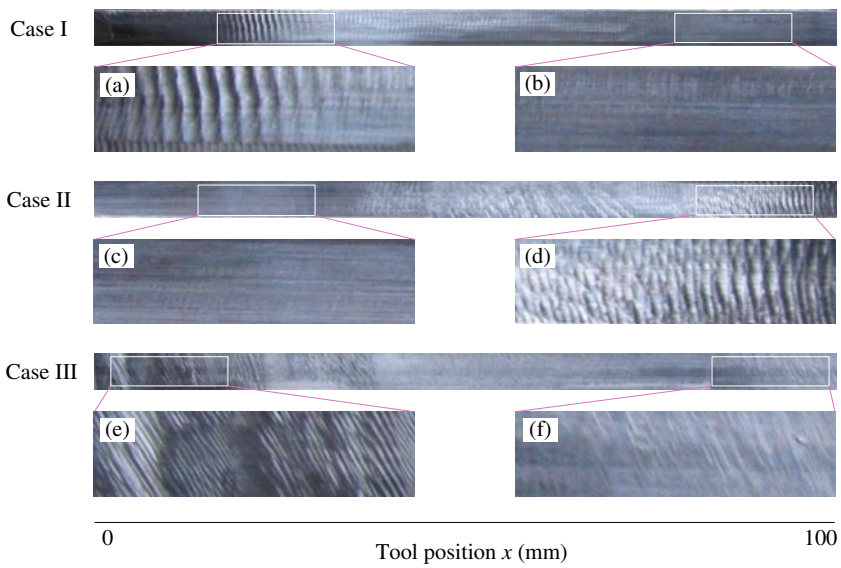

Fig. 6 Photographs of machined workpiece

throughout the machining process. Cutting parameters during machining process of the thin-walled workpiece is selected in order to avoid chatter vibration and increase the chatter-free material removal rate and surface finish.

This work is in progress and will be developed further to include the coupling between tool and workpiece and the end mill with variable pitch. The mode thus obtained will have to be developed with specific software adapted to an industrial context.

Acknowledgments The authors are grateful to the Research Fund for the Doctoral Program of Higher Education of China for supporting this work under grant no. 20100131120030, the Postdoctoral Innovation Foundation of Shandong province for supporting this work under grant no. 200902018, the China Postdoctoral Science Foundation for supporting this work under grant no. 20100481259, and the '973' National Basic Research Program of China for supporting this work under grant no. 2009CB724405.

References

1. Wiercigroch M, Budak E (2001) Sources of nonlinearities, chatter generation and suppression in metal cutting. Phil Trans R Soc Lond A 359:663–693
2. Balachandran B (2001) Nonlinear dynamics of milling processes. Phil Trans R Soc Lond A 359:793–819
3. Tobias SA (1977) Machine tool vibration. China Machine Press, Beijing
4. Smith S, Tlusty J (1990) Update on high-speed milling dynamics. Trans ASME J Eng Ind 112:142–149
5. Altintas Y, Budak E (1995) Analytical prediction of stability lobes in milling. Ann CIRP 44:357–362
6. Davies MA, Pratt JR, Dutterer B, Burns TJ (2002) Stability prediction for low radial immersion milling. Trans ASME J Manuf Sci Eng 124:217–225
7. Faassen RPH, van de Wouw N, Nijimeijer H, Oosterling JAJ (2007) An improved tool path model including periodic delay for chatter prediction in milling. J Comput Nonlinear Dynam 2:167–179
8. Long XH, Balachandran B, Mann BP (2007) Dynamics of milling processes with variable time delays. Nonlinear Dynam 47:49–63
9. Seguy S, Insperger T, Arnaud L, Dessein G, Peigne G (2010) On the stability of high-speed milling with spindle speed variation. Int J Adv Manuf Technol 48:883–895
10. Park SS, Qin YM (2007) Robust regenerative chatter stability in machine tools. Int J Adv Manuf Technol 33:389–402
11. Smith S, Snyder J (2001) A cutting performance based template for spindle dynamics. Ann CIRP 50:259–262
12. Schmitz TL, Davies MA, Medicus K, Snyder J (2001) Improving high-speed machining material removal rates by rapid dynamic analysis. Ann CIRP 50:263–268
13. Tian JF, Hutton SG (2001) Chatter instability in milling systems with flexible rotating spindles—a new theoretical approach. Trans ASME J Manuf Sci Eng 123:1–9
14. Movahhedy MR, Mosaddegh P (2006) Prediction of chatter in high speed milling including gyroscopic effects. Int J Mach Tools Manuf 46:996–1001
15. Chen CK, Tsao YM (2006) A stability analysis of turning a tailstock supported flexible work-piece. Int J Mach Tools Manuf 46:18–25
16. Heisel U, Feinauer A (1999) Dynamic influence on workpiece quality in high speed milling. Ann CIRP 48:321–324
17. Tang AJ, Liu ZQ (2009) Three-dimensional stability lobe and maximum material removal rate in end milling of thin-walled plate. Int J Adv Manuf Technol 43:33–39
18. Davies MA, Balachandran B (2000) Impact dynamics in milling of thin-walled structures. Nonlinear Dynam 22:375–392
19. Bravo U, Altuzarra O, López de Lacalle LN, Sánchez JA, Campa FJ (2005) Stability limits of milling considering the flexibility of the workpiece and the machine. Int J Mach Tools Manuf 45:1669–1680
20. Lan JVL, Marty A, Debongnie JF (2007) Providing stability maps for milling operations. Int J Mach Tools Manuf 47:1493–1496
21. Mane I, Gagnol V, Bouzgarrou BC, Ray P (2008) Stability-based spindle speed control during flexible workpiece high-speed milling. Int J Mach Tools Manuf 48:184–194
22. Thevenot V, Arnaud L, Dessein G, Cazenave-Larroche G (2006) Integration of dynamic behaviour variations in the stability lobes method: 3D lobes construction and application to thin-walled structure milling. Int J Adv Manuf Technol 27:638–644
23. Insperger T, Mann BP, Stépán G, Bayly PV (2003) Stability of up-milling and down-milling, part 1; alternative analytical methods. Int J Mach Tools Manuf 43:25–34
24. Insperger T, Stépán G (2002) Semi-discretization method for delayed systems. Int J Numer Methods Eng 55:503–518
25. Hartung F, Insperger T, Stepan G, Turi J (2006) Approximate stability charts for milling processes using semi-discretization. Appl Math Comput 174:51–73